

## *Electronic Supplementary Information (ESI)*

### **Electron-enriched thione enables strong Pb-S interaction for stabilizing high quality CsPbI<sub>3</sub> perovskite films with low-temperature processing**

Xiaojia Xu,<sup>a</sup> Hao Zhang,<sup>a</sup> Erpeng Li,<sup>a</sup> Pengbin Ru,<sup>b</sup> Han Chen,<sup>b</sup> Zhenhua Chen,<sup>c</sup>  
Yongzhen Wu,<sup>\*a</sup> He Tian <sup>a</sup> and Wei-Hong Zhu <sup>a</sup>

<sup>a</sup> Key Laboratory for Advanced Materials and Joint International Research Laboratory of Precision Chemistry and Molecular Engineering, Feringa Nobel Prize Scientist Joint Research Center, Shanghai Key Laboratory of Functional Materials Chemistry, Institute of Fine Chemicals, School of Chemistry and Molecular Engineering, East China University of Science and Technology, Shanghai 200237, China.

<sup>b</sup> State Key Laboratory of Metal Matrix Composites, Shanghai Jiao Tong University, 800 Dong Chuan Road, Shanghai 200240, China.

<sup>c</sup> Shanghai Synchrotron Radiation Facility (SSRF), Shanghai Advanced Research Institute, Chinese Academy of Sciences, Shanghai 201204, China.

\* E-mail: wu.yongzhen@ecust.edu.cn

## **Contents**

<b>1. Optical spectra of CsPbI<sub>3</sub> films with and without 4-PT .....</b>	<b>2</b>
<b>2. SEM images and EDS mapping of CsPbI<sub>3</sub> films .....</b>	<b>4</b>
<b>4. Thermal stability test of the CsPbI<sub>3</sub> perovskite film .....</b>	<b>5</b>
<b>5. Air stability comparison .....</b>	<b>6</b>
<b>6. Characterization of CsPbI<sub>3</sub> films with different additives .....</b>	<b>6</b>
<b>7. Characterization of the molecular interaction between 4-PT and CsPbI<sub>3</sub> .....</b>	<b>7</b>
<b>9. Synthesis of <i>N</i>-methyl-4-pyridinethione .....</b>	<b>10</b>
<b>10. Notes on the different ESP values of S atoms in additives .....</b>	<b>12</b>

## 1. Optical spectra of CsPbI<sub>3</sub> films with and without 4-PT

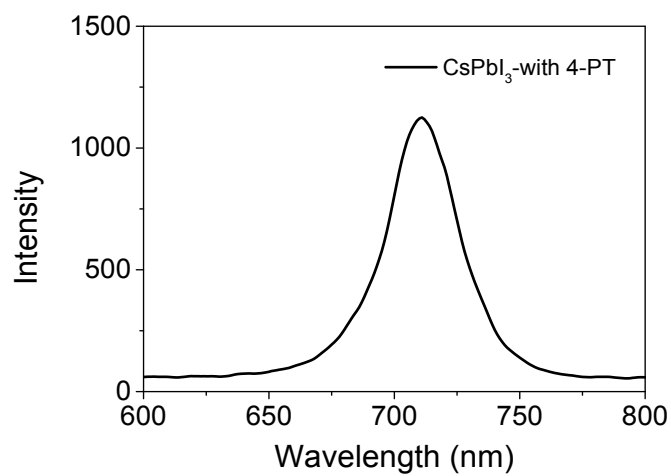


**Fig. S1** PL spectrum of black-phase CsPbI<sub>3</sub> perovskite film stabilized by 4-PT. The excitation wavelength was set as 470 nm.

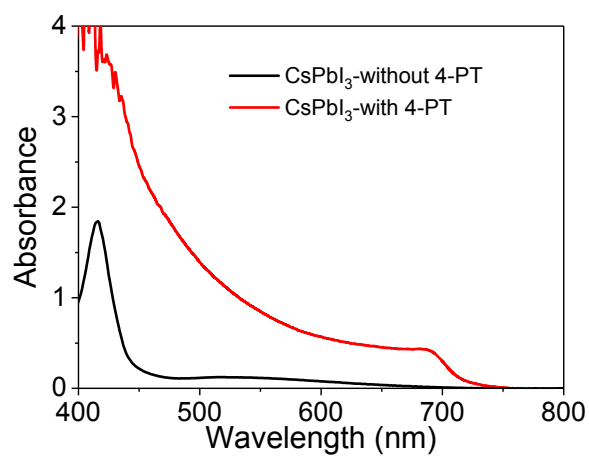


**Fig. S2** Absorption spectra of CsPbI<sub>3</sub> films without or with 4-PT.

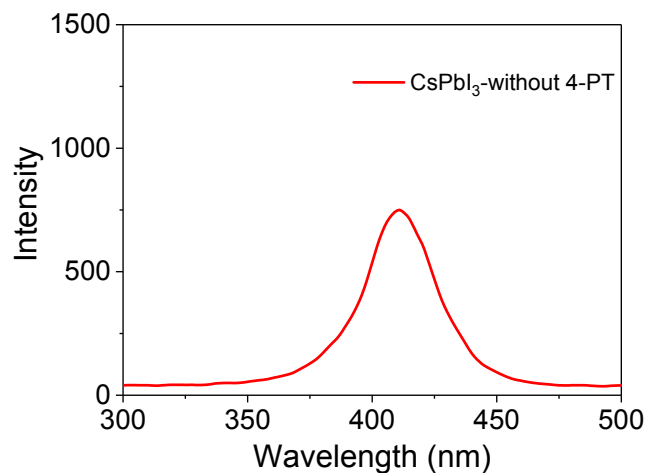


**Fig. S3** PL spectrum of yellow-phase  $\text{CsPbI}_3$  film without 4-PT. The excitation wavelength was set as 300 nm.

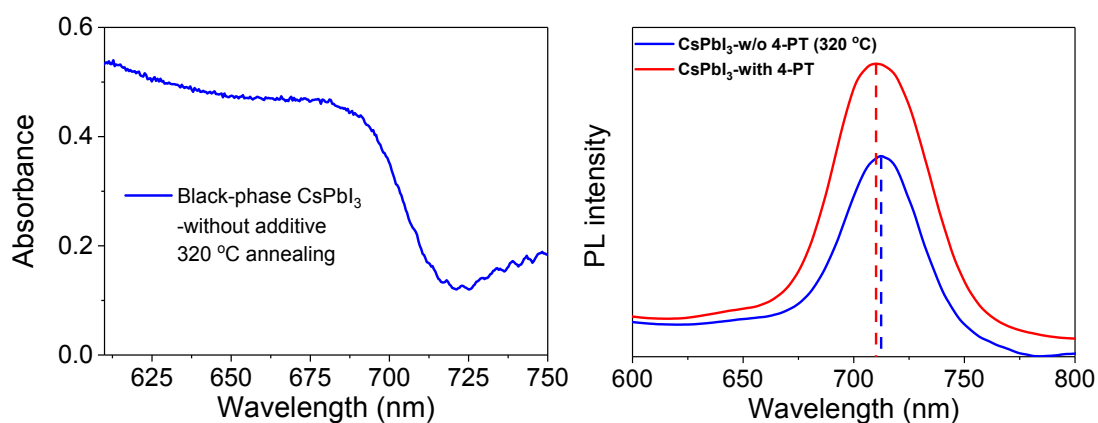


**Fig. S4 Left:** Absorption spectrum of the additive-free black-phase  $\text{CsPbI}_3$  film annealed at 320 °C for 10 minutes. The spectrum was acquired by a homemade optical fiber based in-situ spectroscopy. **Right:** PL spectra of black-phase  $\text{CsPbI}_3$  films with or without 4-PT (excited at 480 nm). The black-phase  $\text{CsPbI}_3$  film without 4-PT was obtained by annealing at 320 °C for 10 minutes.

## 2. SEM images and EDS mapping of CsPbI<sub>3</sub> films

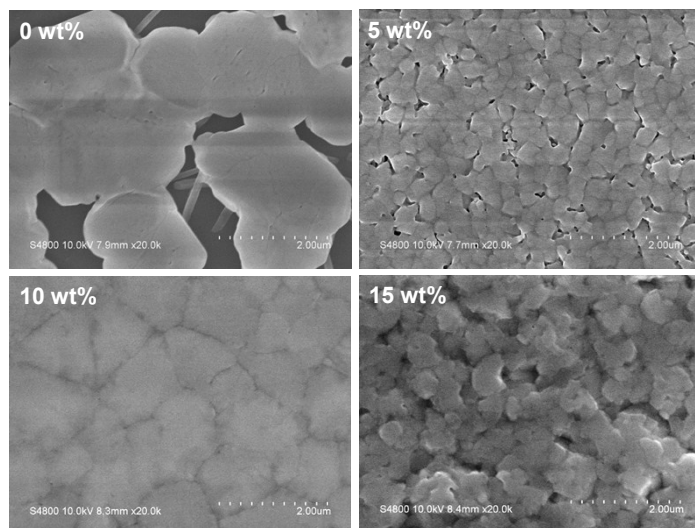


**Fig. S5** SEM images of CsPbI<sub>3</sub> films fabricated with various concentration of 4-PT.

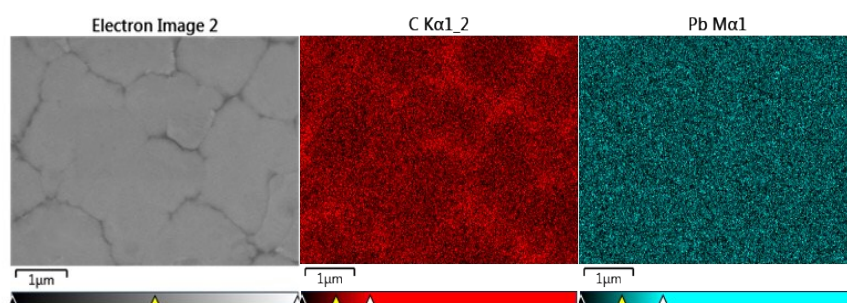


**Fig. S6** EDS mapping C and Pb elements of black-phase CsPbI<sub>3</sub> with 10 wt% 4-PT.

### 3. Retarded crystallization process of the CsPbI<sub>3</sub> film

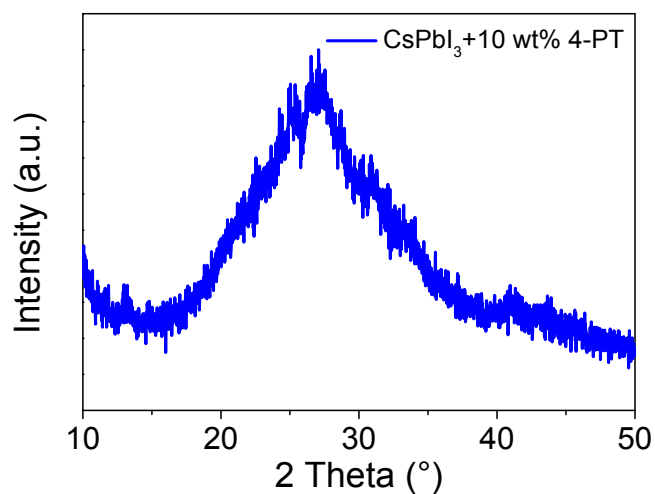


**Fig. S7** XRD pattern of CsPbI<sub>3</sub> film with 10 wt% 4-PT annealed at 50 °C for 5 minutes.

### 4. Thermal stability test of the CsPbI<sub>3</sub> perovskite film

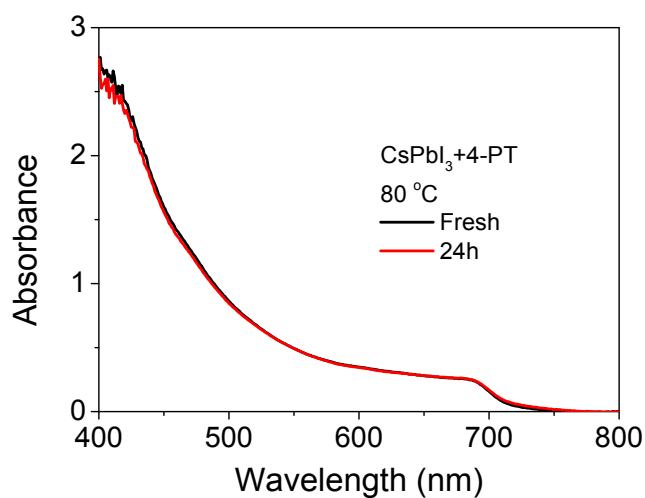


**Fig. S8** Absorption spectra of the CsPbI<sub>3</sub> perovskite film measured immediately after fabrication (Fresh) and aged in nitrogen glove box at 80 °C (24 h).

### 5. Air stability comparison

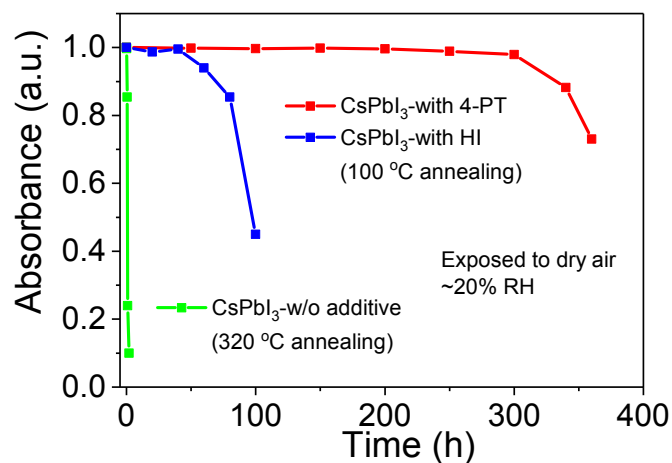


**Fig. S9** Evolution of the absorbance at 690 nm for the additive-free black-phase CsPbI<sub>3</sub> film and the 4-PT or HI based black-phase CsPbI<sub>3</sub> films exposed to air (~20% RH).

## 6. Characterization of CsPbI<sub>3</sub> films with different additives

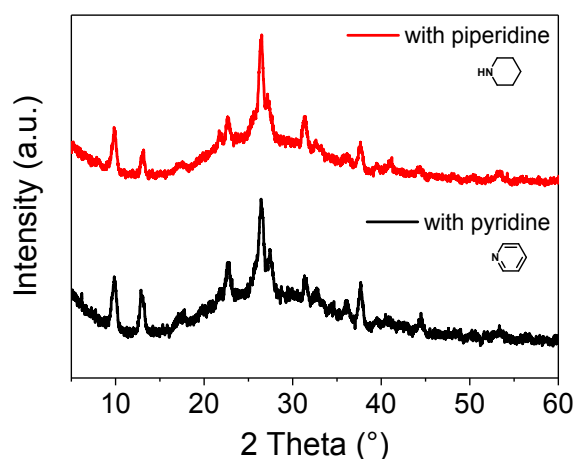


**Fig. S10** XRD patterns of the CsPbI<sub>3</sub> perovskite precursor films with the addition of pyridine and piperidine.

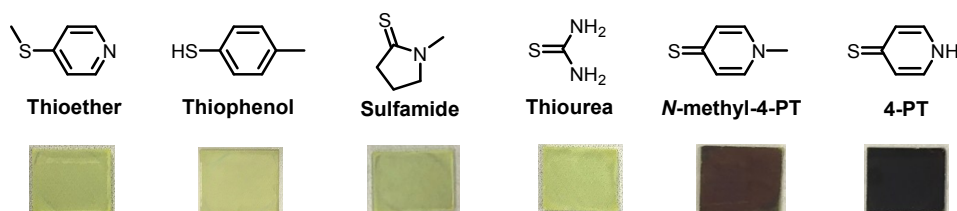


**Fig. S11** Chemical structures of various additives and corresponding photos of CsPbI<sub>3</sub> films after thermal annealing.

## 7. Characterization of the molecular interaction between 4-PT and

## CsPbI<sub>3</sub>

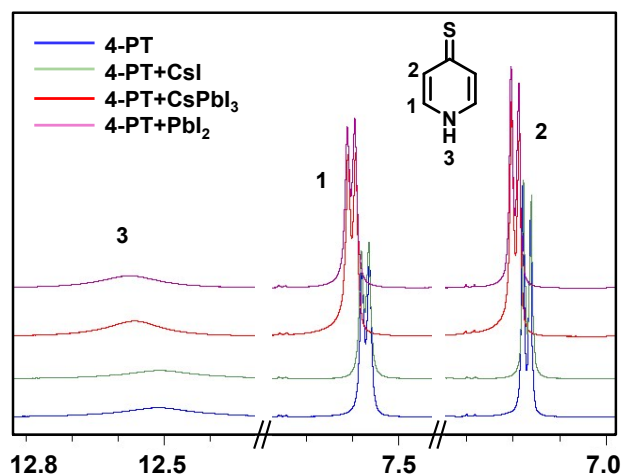


**Fig. S12** <sup>1</sup>H NMR spectra of pure 4-PT, 4-PT mixed with PbI<sub>2</sub>, CsI and CsPbI<sub>3</sub> in DMSO-*d*<sub>6</sub> solution. Specifically, the samples were prepared by dissolving 5 mg pure 4-PT alone, or a mixture of 5 mg 4-PT with perovskite precursor materials (2 mg PbI<sub>2</sub> or 2 mg CsI or 4 mg CsPbI<sub>3</sub>) in DMSO-*d*<sub>6</sub>.

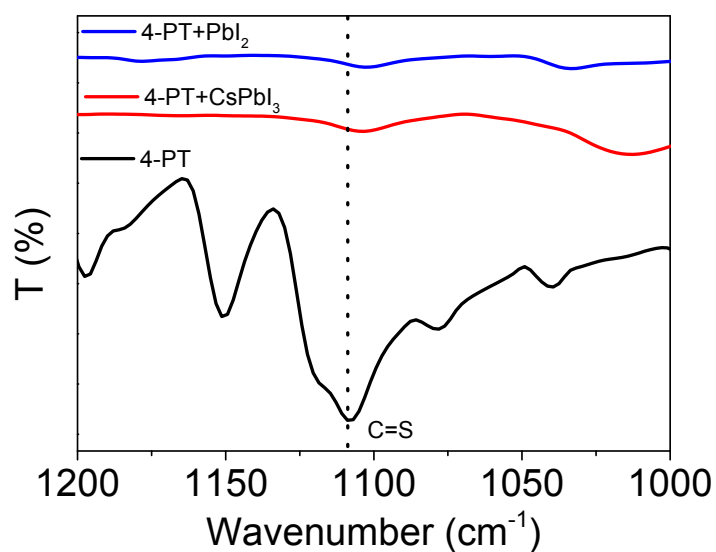


**Fig. S13** Magnified Fourier transform infrared (FTIR) spectra of pure 4-PT, CsPbI<sub>3</sub> and PbI<sub>2</sub> precursor films mixed with 4-PT.

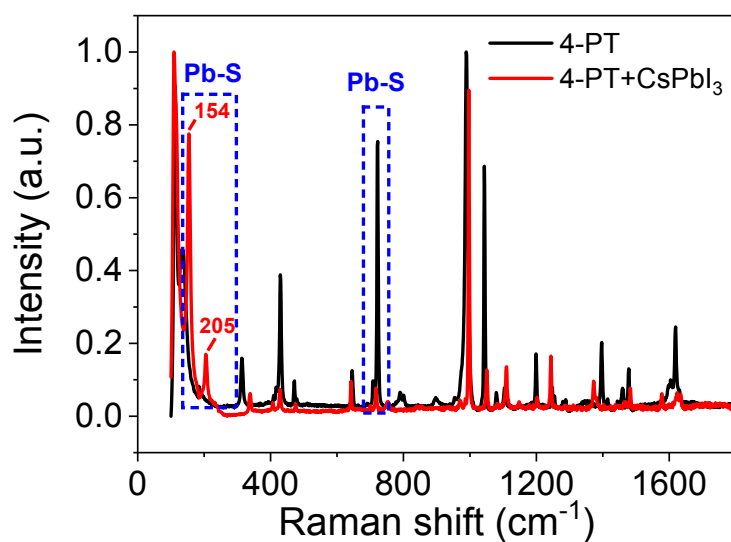


**Fig. S14** Raman spectra of 4-PT and 4-PT with  $\text{CsPbI}_3$  complex. Specifically, the complex was prepared by dissolving 4-PT powder in  $\text{CsPbI}_3$  precursor solution at 0.8 M concentration, then the solution was dripped into large amounts of chlorobenzene to obtain the precipitate. The collected powders were dried in a vacuum oven for 12 h before Raman measurement.

## 8. Device characterization

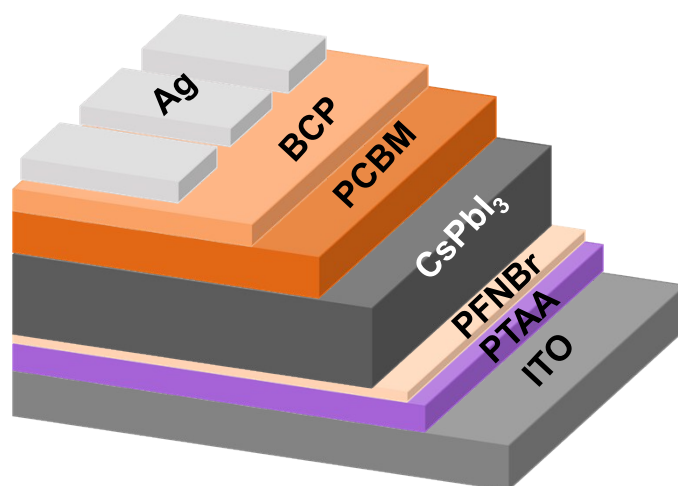


**Fig. S15** Structure of  $\text{CsPbI}_3$  perovskite solar cells.



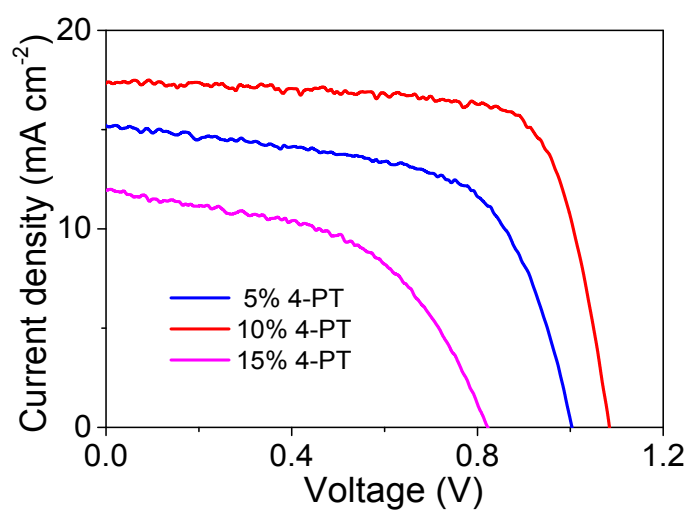


**Fig. S16**  $J$ - $V$  curves of  $\text{CsPbI}_3$  perovskite devices with various concentrations of 4-PT.

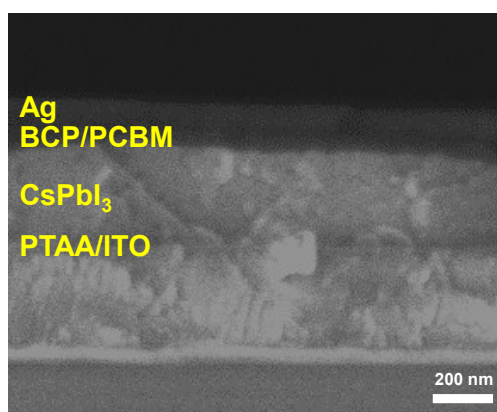


**Fig. S17** Cross-sectional SEM image of  $\text{CsPbI}_3$  device stabilized by 10 wt% 4-PT.

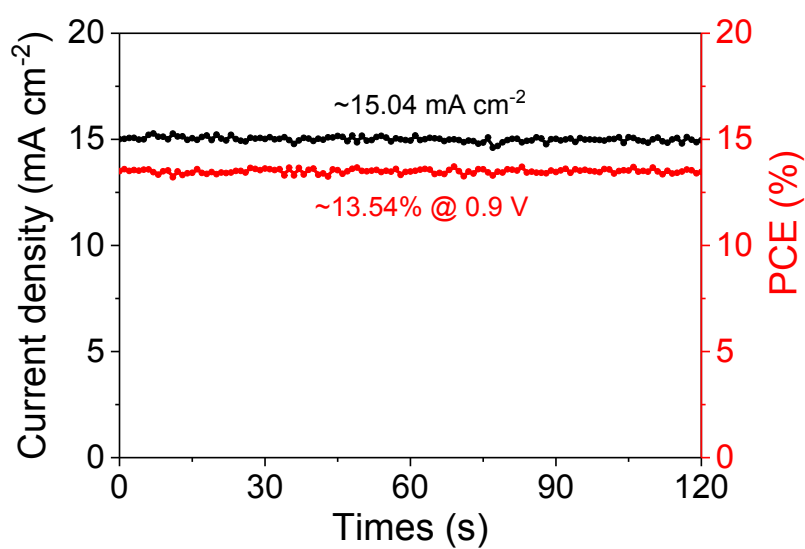
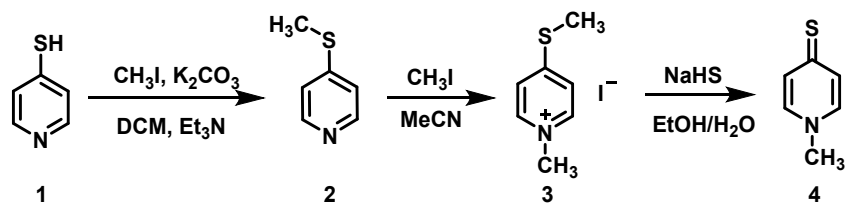


**Fig. S18** Steady-state photocurrent and stabilized power output of the most efficient device.

## 9. Synthesis of *N*-methyl-4-pyridinethione



**Scheme S1** Synthetic Route of *N*-methyl-4-pyridinethione.

*N*-methyl-4-pyridinethione is prepared according to previously reported method<sup>1</sup>.<sup>2</sup> The synthetic route is shown in **Scheme S1**, which involves commercially available low-cost raw materials in three-step reactions. Specifically, the starting material **1** (3.66 mmol, 0.41 g),  $\text{K}_2\text{CO}_3$  (7.32 mmol, 1.01 g),  $\text{CH}_2\text{Cl}_2$  (15 mL) were added to a round-bottom flask and stirred at 0 °C for 5 minutes. To this mixture,  $\text{CH}_3\text{I}$  (5.49 mmol, 0.35 ml) was added, followed by  $\text{Et}_3\text{N}$  (0.5 ml). After stirring at room temperature for 5-6 h, the reaction mixtures were extracted with  $\text{CH}_2\text{Cl}_2$  ( $3 \times 10$  ml). The organic phases were combined together, dried over anhydrous  $\text{Na}_2\text{SO}_4$  and purified by silica gel chromatography (pure  $\text{CH}_2\text{Cl}_2$ ) to give yellow liquid **2** in about 45% yield (1.63 mmol, 0.20 g).  $^1\text{H}$  NMR (400 MHz,  $\text{CDCl}_3$ , ppm): 8.38 (dd,  $J_1 = 6.0$  Hz,  $J_2 = 3.2$  Hz, 2 H), 7.09 (dd,  $J_1 = 6.4$  Hz,  $J_2 = 2.8$  Hz, 2 H), 2.48 (s, 3 H).

Then, in a round-bottom flask, the intermediate **2** (1.51 mmol, 0.19 g) and  $\text{CH}_3\text{I}$  (2.27 mmol, 0.32 g) were dissolved in  $\text{CH}_3\text{CN}$  (8.5 mL). The mixture was stirred at room temperature overnight and then dropped into ether solution. After that, the precipitate was filtered off and vacuum dried to obtain white powder **3** (1.14 mmol, 0.30 g). Yield: 75%. Finally, **3** (1.10 mmol, 0.29 g),  $\text{NaHS}$  (2.31 mmol, 0.13 g) was added to a solution of  $\text{EtOH}/\text{H}_2\text{O}$  (5.5 mL, 1/1: v/v), the mixture was stirred at room temperature for 5-6 h. The resulting mixture was extracted with  $\text{CH}_2\text{Cl}_2$  ( $3 \times 10$  ml) and the organic phases were combined, dried with  $\text{Na}_2\text{SO}_4$  and purification by silica gel chromatography ( $\text{CH}_2\text{Cl}_2$ :  $\text{CH}_3\text{OH}$  = 50: 1) to afford yellow powder **4**. The resulting powder was further vacuum dried and resulted in about 47% yield (0.52 mmol, 0.06 g).  $^1\text{H}$  NMR (400 MHz,  $\text{CDCl}_3$ , ppm): 7.42 (d,  $J = 7.2$  Hz, 2 H), 7.09 (d,  $J = 6.8$  Hz, 2 H), 3.73 (s, 3 H).

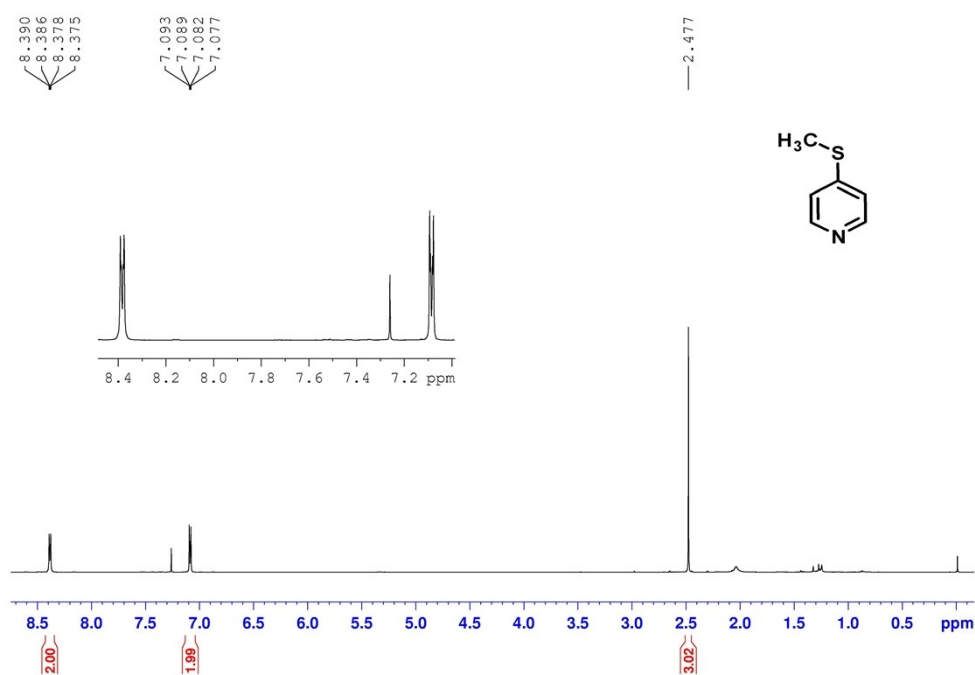


**Fig. S19**  $^1\text{H}$  NMR of *S*-methyl-4-mercaptopyridine recorded in  $\text{CDCl}_3$ .

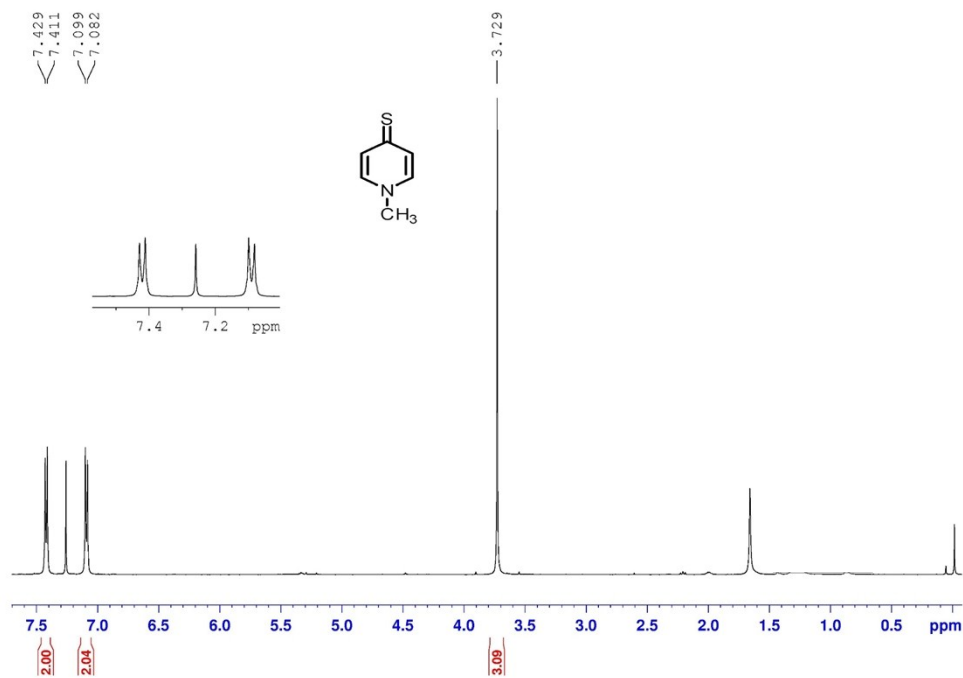


**Fig. S20**  $^1\text{H}$  NMR of *N*-methyl-4-pyridinethione recorded in  $\text{CDCl}_3$ .

## 10. Notes on the different ESP values of S atoms in additives

Compared to thione based additives, thioether and thiophenol lack the resonant assistance of N lone pair electrons, therefore the electron density of S atoms mainly originates from their lone pair electrons. For sulfamide and thiourea, they both have C=S double bond and adjacent N atoms. The lone pair electrons of N atom can conjugate with C=S double bond thus increases the electron density of S atoms. Compared to sulfamide, thiourea has two adjacent N atoms, therefore making the electron density of S atom higher than that in sulfamide. We can draw this conclusion easily by writing the resonance formula as shown in **Fig. S21**.

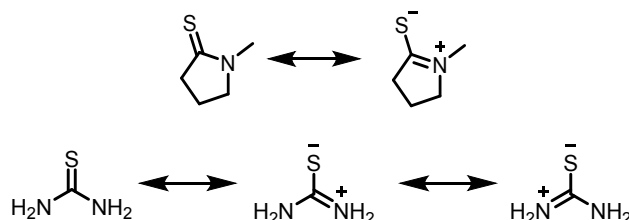


**Fig. S21** The resonance formulas of sulfamide and thiourea structure.

In the pyridinethione based molecule of 4-PT (*N*-methyl-4-PT), the N atom adopts  $sp^2$  hybridization to form covalent bonds with two C and one H ( $-CH_3$ ) in the same plane, and its lone pair electrons will occupy the un-hybridized p orbital. In this case, the resonance of the C=S double bond to form a carbocation and a sulfur anion (as depicted in **Fig. S22**) will be beneficial to stabilize the six-membered ring structure, as the total number of their p orbital electrons becomes 6, which satisfies the Huckel's rule to obtain an aromatic structure. This might be the origin of the lowest ESP for S atoms in the pyridinethione based compounds.

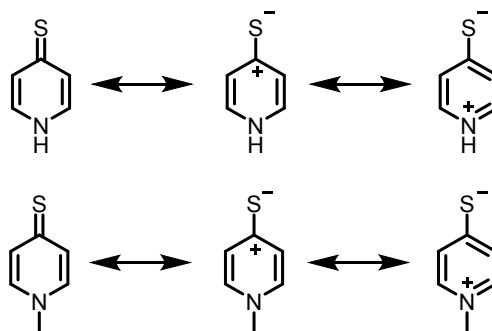


**Fig. S22** The resonance formulas of pyridinethione.

## References:

1. A. L. M. Porto, F. Cassiola, S. L. P. Dias, I. Joekes, Y. Gushikem, J. A. R. Rodrigues, P. J. S. Moran, G. P. Manfio and A. J. Marsaioli, *J. Mol. Catal. B-Enzym.*, 2002, **19-20**, 327-334.
2. J. Levillain, D. Paquer, A. Sene and M. Vazeux, *Synthesis*, 1998, **1998**, 99-104.